Near-Zero Modal-Dispersion (NEMO) Coupled-Core Multi-Core Fibers

Cristian Antonelli, *Senior Member, IEEE, Fellow, OSA*, and Antonio Mecozzi, *Fellow, IEEE, Fellow, OSA*

***Abstract*—We propose a design for coupled-core multi-core fibers that allows to achieve extremely low levels of modal dispersion. These fibers, which we dub *NEar-zero MOdal-dispersion* (NEMO) fibers, have an even number of cores regularly distributed on a circle, and the optimal design parameters follow from a simple condition independent of the number of cores. The modal-dispersion reduction trades off some of the fiber mode-mixing effectiveness, yet without compromising its beneficial property of mitigating nonlinear signal distortions. The semi-analytical tool developed for this study allows to effectively characterize the effect of various types of perturbations to the ideal fiber structure.**

***Index Terms*—Space-division multiplexing, modal dispersion, optical fiber communication, MIMO systems.**

I. Introduction

MULTI-CORE fibers (MCFs) for Space-Division Multiplexed (SDM) transmission allow simultaneous signaling in multiple spatial channels, and, depending on the inter-core distance, the extraction of the transmitted information may or may not require resorting to multiple-input multiple-output (MIMO) digital signal processing (DSP) techniques at the receiver. In coupled-core MCFs the cores are arranged rather closely to each other, so that the fields propagating in the individual cores couple to each other to a non-negligible extent [1]. For suitable values of the core-to-core distances, inter-core coupling takes the form of a random process, owing to the fact that the perturbations to the ideal fiber structure take over the deterministic coupling dictated by coupled-mode theory [2], [3]. The random coupling between cores is known to be beneficial for two main reasons. On the one hand, it reduces the nonlinear signal distortions arising at large optical power levels in fiber-communication systems, compared to the case of single-mode systems [4]–[7]. On the other hand, it reduces the accumulation of the fiber modal dispersion (MD) with the fiber length [8]–[10], as compared to the case in which inter-core coupling is purely deterministic (that is, in the absence of random perturbations). In particular, random mode coupling reduces the growth of MD from linear to square-root with respect to propagation distance. This reduction is of paramount importance, as MD is responsible for aggravating the MIMO-DSP complexity in the process of extracting the transmitted signals at the receiver. For this reason, MD is often considered as a major obstacle towards the implementation of SDM transmission in coupled MCFs. The record-low values of MD, measured on rollable 2-core fiber ribbons [11] and on 4-core fibers deployed in the SDM fiber testbed in L'Aquila (Italy) [12] are of 1.5 $\mathrm{ps}/\sqrt{\mathrm{km}}$ and 2.5 $\mathrm{ps}/\sqrt{\mathrm{km}}$, respectively, two orders of magnitude larger than polarization-mode dispersion (PMD) values around 0.02 $\mathrm{ps}/\sqrt{\mathrm{km}}$ of modern low-PMD fibers.

An important point that should be stressed is that the regime of strong mode mixing is achieved for a suitable fiber design, by properly balancing the various fiber parameters, which include the distance between the cores, their sizes, and their refractive index profiles (which results in changing the cores' propagation constants). Outside of this range of parameters, mode coupling looses its random nature and MD grows linearly with propagation distance. The transition between the two regimes can be seen by varying the distance between the fiber cores and constitutes well-established knowledge in the design of MCFs ([1] and references therein). On the other hand, within the range of parameters for which the fields in the fiber cores evolve in the regime of random mixing, there is room for optimizing the fiber design with the goal of reducing MD. While this optimization is key to deploy practical CC-MCF transmission, all reported studies, to the best of the authors' knowledge, are limited to considering only the effect of varying the distance between homogeneous cores [10], [13]–[16]. Indeed, the consideration of homogeneous cores only is reasonably justified with reference to the design of weakly-coupled MFCs, where some inhomogeneity between cores is introduced as a means of reducing inter-core crosstalk.

In this work we propose a fiber design that aims to reducing MD by optimizing not only the core pitch, but also the individual cores propagation constants. We find that by arranging an even number of inhomogeneous cores on a circles, so that each core is coupled to two identical cores with the same propagation-constant mismatch, allows, for a suitable parameter choice, a substantial reduction of the fiber MD. The optimal design implies a balance between the frequency dependence of the propagation-constant mismatch and that of the inter-core

Manuscript received July 21, 2021; revised September 8, 2021; accepted September 21, 2021. Date of publication September 28, 2021; date of current version December 2, 2021. This work was supported by the Italian Government through project Innovating City Planning through Information Communication Technologies (INCIPICT), and PRIN 2017 project Fiber Infrastructure for Research on Space-Division Multiplexed Transmission (FIRST). *(Corresponding author: Cristian Antonelli.)*

Cristian Antonelli and Antonio Mecozzi are with the Department of Physical and Chemical Sciences, University of L'Aquila, 67100 L'Aquila, Italy, and also with the National Laboratory of Advanced Optical Fibers for Photonics (FIBERS), CNIT 67100, Italy (e-mail: cristian.antonelli@univaq.it; antonio.mecozzi@univaq.it).

Color versions of one or more figures in this article are available at https://doi.org/10.1109/JLT.2021.3115912.

Digital Object Identifier 10.1109/JLT.2021.3115912

coupling coefficient. Our study shows that for fibers with four to eight cores the MD coefficient can be reduced to values of the order of 0.1 $\mathrm{ps}/\sqrt{\mathrm{km}}$, typical of legacy single-mode fibers' PMD, and more than one order of magnitude lower than record-low MD values [11], [12]. This value reduces to about 0.04 $\mathrm{ps}/\sqrt{\mathrm{km}}$ in the case of a two-core fiber. We dub this fiber design *NEar-zero MOdal dispersion* (NEMO). The study of MD in NEMO fibers relies on the evolution of the semi-analytical tool introduced in [17], and its accuracy is tested against numerical results. We show that random coupling in NEMO fibers occurs on the scale of hundreds of meters to a kilometer, longer than in homogeneous MCFs, but still sufficiently short to mitigate nonlinear distortions.

II. NEMO Multi-Core Fiber Design

We start by considering the case of a fiber with two inhomogeneous single-mode cores. In the absence of perturbations to the ideal fiber structure, a scalar (single-polarization) description of the electric fields in the two cores is appropriate, and their evolution is described by the following coupled equations,

$$\frac{\mathrm{d}E_1}{\mathrm{d}z} = i\frac{\Delta\beta}{2}E_1 + i\kappa E_2 \tag{1}$$

$$\frac{\mathrm{d}E_2}{\mathrm{d}z} = i\kappa E_1 - i\frac{\Delta\beta}{2}E_2, \tag{2}$$

where $\Delta\beta$ is the propagation-constant mismatch between the two cores and κ is the coupling coefficient [18]. There is a one-to-one correspondence between these equations and the equations describing propagation in a single-mode fiber in the presence of constant birefringence, where the birefringence vector is given by [19] $\vec{b} = \Delta\beta\hat{e}_1 + 2\kappa\hat{e}_2$, that is

$$\frac{\mathrm{d}\vec{E}}{\mathrm{d}z} = i\frac{\vec{b}\cdot\vec{\sigma}}{2}\vec{E}, \tag{3}$$

where $\vec{E}$ is a Jones vector with components E_1 and E_2, and where $\vec{\sigma}$ is a three-dimensional vector whose components are the familiar Pauli matrices [19]. Within this analogy, the modal dispersion affecting the coupled-core fiber can be described in terms of the resulting PMD vector, which can be shown to be given by $\vec{\tau} = b_\omega \hat{b} z$ with $b = |\vec{b}|$ and $\hat{b} = \vec{b}/b$. The coupled-core fiber is therefore MD-free for $\vec{\tau} = 0$, which implies $b_\omega = 0$, or equivalently for

$$\vec{b}\cdot\vec{b}_\omega = \Delta\beta\Delta\beta_\omega + 4\kappa\kappa_\omega = 0. \tag{4}$$

Heuristically, the above condition can be interpreted as a balancing between the intra-core dispersion and the dispersion of the inter-core coupling. The existence of a set of fiber parameters for which the above condition is fulfilled is plausible in all relevant cases. In fact, on the one hand, $\Delta\beta$ and $\Delta\beta_\omega$ are of the same sign (and hence their product is positive), as can be seen by inspecting the dispersion diagram of linearly-polarized modes in a step-index fiber for values of the normalized frequency below the single-mode cut-off of 2.405 [20]. On the other hand, κ_ω is negative-valued, as follows from the fact that the mode size reduces with the increasing frequency, and so does the overlap integral between the modes of the two cores, to which κ is proportional. We notice that the expression $\vec{\tau} = b_\omega \hat{b} z$ is identical to the expression of the PMD vector derived for twisted fibers with uniform birefringence in [21], where it was also found that PMD vanishes for $\vec{b}\cdot\vec{b}_\omega = 0$.

We now move to accounting for the effect of random polarization-mode coupling within each of the two fiber cores. This mechanism is responsible for producing strong random mixing between the fields in the two cores, and the fiber MD can be characterized in terms of the intensity impulse response duration T [3], [22], [23]. In the regime of strong mode mixing, T grows proportionally to the propagation distance square-root [23], as

$$T = \kappa_{\mathrm{MD}}\sqrt{z}, \tag{5}$$

where κ_{MD} is what we refer to as the MD coefficient [17], [23]. The propagation equations for the Jones vectors $\vec{E}_1$ and $\vec{E}_2$ describing the fields in the two cores are

$$\frac{\mathrm{d}\vec{E}_1}{\mathrm{d}z} = -i\frac{\Delta\beta}{2}\vec{E}_1 + i\frac{\vec{\beta}_1\cdot\vec{\sigma}}{2}\vec{E}_1 + i\kappa\vec{E}_2 \tag{6}$$

$$\frac{\mathrm{d}\vec{E}_2}{\mathrm{d}z} = i\frac{\Delta\beta}{2}\vec{E}_2 + i\frac{\vec{\beta}_2\cdot\vec{\sigma}}{2}\vec{E}_2 + i\kappa\vec{E}_1, \tag{7}$$

where $\vec{\beta}_1$ and $\vec{\beta}_2$ are the birefringence vectors of the two cores [19]. For this study we assume that they are isotropic Gaussian vectors independent of each other (which reflects the idea that random mode coupling occurs independently in the two cores) with the following correlation function

$$\langle\vec{\beta}_n(z)\cdot\vec{\beta}_n(z')\rangle = \left(\frac{2\pi}{L_B}\right)^2 e^{-\frac{|z-z'|}{L_C}} \ (n=1,2), \tag{8}$$

where L_C is the birefringence correlation length and L_B is the beat length. The extraction of κ_{MD} is based on the procedure introduced in [17], as discussed in Sec. III. In Fig. 1 we plot the MD coefficient κ_{MD} as a function of the coupling coefficient κ, which is varied by varying the core-to-core distance. The curves correspond to the values of $\Delta\beta = \beta - \beta_0$ shown in the legend, which were obtained by slightly increasing the radius of one core, while keeping that of the other core fixed at a reference value corresponding to the propagation constant $\beta_0 \simeq 5.83\times10^6$ m^{-1}. The numerical details are provided in Sec. V. The birefringence beat length was set to $L_B = 1$ m and the correlation length to $L_C = 0.1$ m. Note that the value of L_B is consistent with recent measurements of the beat length in deployed MCFs [24], while we can only speculate that of L_C based on studies of single-mode fibers [25], as experimental data are not yet available. The lower panel shows a plot of the quantity $\Delta\beta\Delta\beta_\omega + 4\kappa\kappa_\omega$, to which the scalar product $\vec{b}\cdot\vec{b}_\omega$ is proportional,

$$\vec{b}\cdot\vec{b}_\omega = 4(\Delta\beta\Delta\beta_\omega + 4\kappa\kappa_\omega), \tag{9}$$

where by the vector $\vec{b}$ we now denote the generalized birefringence vector that describes deterministic coupling in a two-mode fiber [9] (indeed in Eq. (9) $\vec{b}$ denotes a generalized 15-dimensional Stokes vector, while in Eq. (4) it denotes a 3-dimensional Stokes vector). The figure shows that the MD coefficient is vanishing in correspondence of core-pitch values

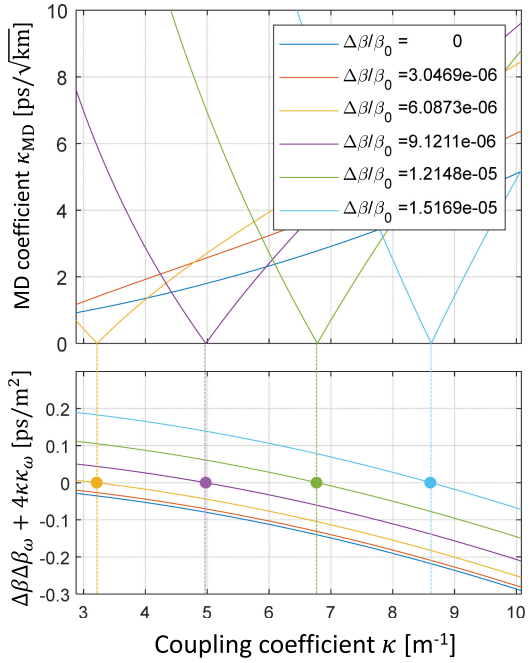

Fig. 1. The top panel shows the MD coefficient $\kappa_{\rm MD}$ as a function of the coupling coefficient κ for a two-core NEMO fibers. The various curves refer to the displayed values of the propagation-constant mismatch $\Delta\beta$. Correspondingly, the lower panel shows a plot of Eq. (9).

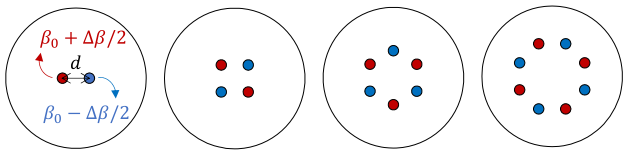

Fig. 2. The proposed NEMO design rule. The cores are arranged in a ring configuration, and the red-filled cores have a propagation constant higher by $\Delta\beta$ than the blue-filled cores. The cladding diameter, cores' average radius, and core-to-core distance d are proportional to 125 μm, 4.6 μm, and 24 μm, respectively.

for which $\vec{b}\cdot\vec{b}_\omega \simeq 0$ (independently of the magnitude of L_B and L_C, as we checked). This finding is somehow surprising, and seems to follow from the absence of dispersion in the ideal case where the fiber cores are not affected by random polarization-mode coupling.

We now move to discussing the extension of the proposed design to larger core counts. The driving idea is that if each core is coupled to two other cores with a propagation constant either greater or smaller by $\Delta\beta$, then modal dispersion may accumulate similarly to how it accumulates in the two-core fiber. This design rule can be implemented for even numbers of cores in a ring configuration, as sketched in Fig. 2, provided that the fiber cladding be sufficiently large, as is the case for up to eight cores in a 125-μm cladding diameter.[1]

Fig. 3 shows the results for four-, six-, and eight-core NEMO fibers. Compared to the case of a two-core fiber, it can be

[1]The case of eight cores is border-line. In fact, for a core pitch of 24 μm, the distance of the cores from the cladding edge is about 6.8 times the core radius, while it should be almost 8 times for a confinement loss of 10^{-3} dB/km and about 7 times for 10^{-2} dB/km, as calculated for the 10-core fiber of [26]. This may require a slightly larger cladding diameter than 125 μm.

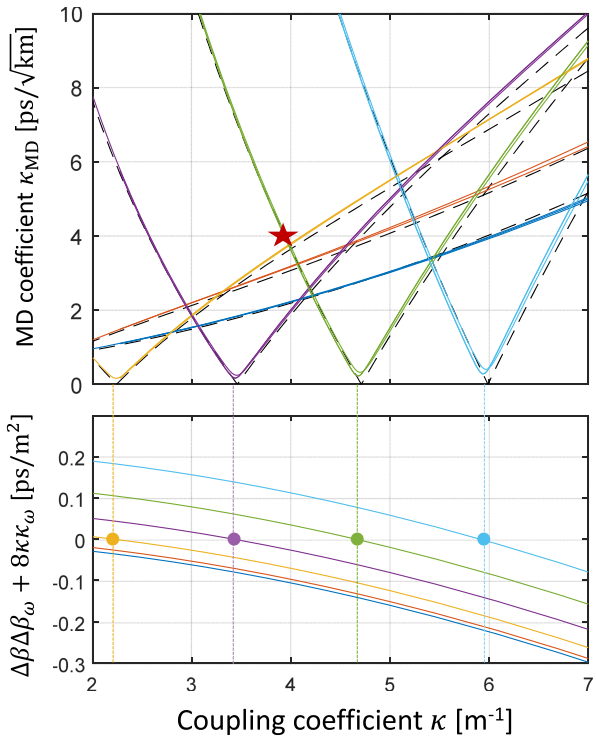

Fig. 3. The solid curves in the top panel shows the MD coefficient $\kappa_{\rm MD}$ as a function of the coupling coefficient κ for NEMO fibers with four, six, and eight cores, for the same values of the propagation-constant mismatch of Fig. 1. The dashed curves are re-drawn from Fig. 1, except that they are plotted versus $\kappa/\sqrt{2}$. Correspondingly, the lower panel shows a plot of Eq. (10). Different colors refer to different values of $\Delta\beta$, according to the same color code as in Fig. 1.

seen that the main result is preserved, namely MD reduces drastically, for the optimal coupling coefficients, to values of the order of $0.1\ \mathrm{ps}/\sqrt{\mathrm{km}}$ – one order of magnitude smaller than the record-low value of $2.5\ \mathrm{ps}/\sqrt{\mathrm{km}}$ measured in L'Aquila MCF test-bed [12]. The main difference between the two cases is in the smaller values of the optimal coupling coefficients. These values fulfill approximately the equation $\Delta\beta\Delta\beta_\omega + 8\kappa\kappa_\omega \simeq 0$, as is seen in the lower panel. Like in the case of the two-core fiber, the quantity $\Delta\beta\Delta\beta_\omega + 8\kappa\kappa_\omega$ is proportional to the scalar product $\vec{b}\cdot\vec{b}_\omega$, which reads as (see Sec. III for the details)

$$\vec{b}\cdot\vec{b}_\omega = N^2(\Delta\beta\Delta\beta_\omega + 8\kappa\kappa_\omega). \tag{10}$$

The important difference between the above and Eq. (9) is in a factor of eight versus the factor of four preceding the term $\kappa\kappa_\omega$, which can be heuristically interpreted as a doubling of inter-core coupling dispersion due to the fact that each core couples to two other cores rather than one. Notice that the MD coefficient is approximately the same in all cases. In the same figure, by dashed curves we plot the curves of Fig. (1) versus $\kappa/\sqrt{2}$. As is evident from the figure, when plotted versus the re-scaled coupling coefficient, the results for the two-core fiber essentially overlap with those obtained for four and more cores. This scaling is key to developing an understanding of the NEMO design, and is discussed in Sec. II-A.

Fig. 4 provides a visual illustration of the MD reduction studied in Fig. 3. Plotted in the figure is the intensity waveform

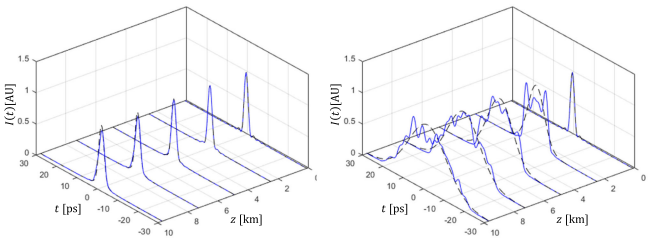

Fig. 4. The propagating intensity waveform in a four-core NEMO fiber for an input frequency-flat signal of 400-GHz optical bandwidth (details in Sec. III). The left and right panels refer to the optimal settings around $\kappa \simeq 4.7$ m^{-1} of Fig. 3 and to the settings pinpointed with a star in the same figure, respectively. The dashed curves show the theory, while the solid curves show numerical simulations.

$I(t)$ propagating in a four-core NEMO fiber corresponding to a frequency-flat input waveform of 400-GHz optical bandwidth (the definition of $I(t)$ and its relation with the intensity impulse response are discussed in Section III). The left panel refers to the optimal settings around $\kappa \simeq 4.7$ m^{-1} of Fig. 3, while the right panel refers to the settings pinpointed with a star in the same figure. Dashed and solid curves show theory and numerical simulations, respectively.

A. Simple Rule for Scaling From 2 to N Cores

The case of more than two cores is described by coupled equations that are a straightforward extension of Eqs. (6)–(7),

$$\frac{\mathrm{d}\vec{E}_{2n-1}}{\mathrm{d}z} = -i\frac{\Delta\beta}{2}\vec{E}_{2n-1} + i\frac{\vec{\beta}_{2n-1}\cdot\vec{\sigma}}{2}\vec{E}_{2n-1} + i\kappa\vec{E}_{2n-2} + i\kappa\vec{E}_{2n} \tag{11}$$

$$\frac{\mathrm{d}\vec{E}_{2n}}{\mathrm{d}z} = i\frac{\Delta\beta}{2}\vec{E}_{2n} + i\frac{\vec{\beta}_{2n}\cdot\vec{\sigma}}{2}\vec{E}_{2n} + i\kappa\vec{E}_{2n-1} + i\kappa\vec{E}_{2n+1}, \tag{12}$$

with $n = 1\cdots N/2$, $\vec{E}_{N+1} = \vec{E}_1$ and $\vec{E}_0 = \vec{E}_N$. It should be noted that since the cores are not identical and their fundamental modes do not form an orthogonal basis for the electromagnetic field, the coupling coefficients should be slightly modified as prescribed by the nonorthogonal coupled-mode theory [27]. However, as will be clear in what follows, the cores are nearly identical and sufficiently separated, so that the small corrections to the orthogonal coupled-mode theory can be ignored. In fact, for the smallest core pitch considered in this work, these corrections would result in a negligible change in the coupling coefficients between nearest-neighboring cores and a non-zero coupling between second-neighboring cores with coupling coefficients that are about three orders of magnitude smaller than the coupling coefficients between nearest neighbors.

The key-point is expressing the electric field vectors in the *odd* (i.e. with odd subscripts) and *even* (i.e. with even subscripts) cores in terms of their discrete Fourier transforms $\vec{V}_h$ and $\vec{U}_h$, respectively,

$$\vec{E}_{2n-1} = \sum_{h=1}^{N/2} \exp\left(ih\frac{4\pi}{N}n\right)\vec{V}_h \tag{13}$$

$$\vec{E}_{2n} = \sum_{h=1}^{N/2} \exp\left(ih\frac{4\pi}{N}n\right)\vec{U}_h, \tag{14}$$

which form an alternative orthogonal basis for the expressing the electric fields in the individual cores. This changes the coupled equations in the form

$$\frac{\mathrm{d}\vec{V}_h}{\mathrm{d}z} = -i\frac{\Delta\beta}{2}\vec{V}_h + i\sum_{k=1}^{N/2}\frac{\vec{\beta}^{(V)}_{h-k}\cdot\vec{\sigma}}{N}\vec{V}_k + i\kappa\left[1+\exp\left(i\frac{4\pi}{N}h\right)\right]\vec{U}_h \tag{15}$$

$$\frac{\mathrm{d}\vec{U}_h}{\mathrm{d}z} = i\frac{\Delta\beta}{2}\vec{U}_h + i\sum_{k=1}^{N/2}\frac{\vec{\beta}^{(U)}_{h-k}\cdot\vec{\sigma}}{N}\vec{U}_k + i\kappa\left[1+\exp\left(-i\frac{4\pi}{N}h\right)\right]\vec{V}_h, \tag{16}$$

where by $\vec{\beta}^{(V)}_h$ and $\vec{\beta}^{(U)}_h$ we denote the discrete Fourier transforms of $\vec{\beta}_{2n-1}$ and $\vec{\beta}_{2n}$, respectively. The new set of equations shows that the Fourier modes form two groups of degenerate modes with a propagation-constant mismatch equal to $\Delta\beta$, where all modes belonging to the same group are strongly coupled in a random fashion (as implied by the summations in Eqs. (15) and (16)). Notice that this phenomenology describes what happens within even cores, as well as within odd cores, thereby establishing a similarity with the coupling dynamics between any two non-degenerate mode groups of few-mode fibers, like LP_{01} and LP_{11} [28]. While the Fourier decomposition provides a clear explanation for the rapid mixing within odd and even cores, it is interesting to point out that this mixing takes place in spite of the fact that odd and even cores are not nearest neighbors, a phenomenon that reminds the tunneling effect in quantum mechanics. On the other hand, the h-th mode of one group is deterministically coupled to the h-th mode of the other group through the coefficient $\kappa[1+\exp(i4\pi h/N)]$, and it may be shown[2] that local power coupling is characterized by the squared modulus of this coefficient, that is $2\kappa^2 + 2\kappa^2\cos(4\pi h/N)$. The core-averaged local power coupling is in turn characterized by the average of these coefficients, which is equal to $2\kappa^2 + 2\kappa^2 N^{-1}\sum_{h=1}^{N/2}\cos(4\pi h/N) = 2\kappa^2$. The corresponding coefficient for a two-core NEMO fiber is instead κ^2. This argument suggests that the evolution of the modal content in a NEMO fiber with N cores is equivalent to that of a fiber with 2 cores with a coupling coefficient greater by a factor of $\sqrt{2}$. This provides an intuitive understanding of the difference between Eqs. (9) and (10)

In the top panel of Fig. 5 by solid curves we plot the average value of the (normalized) total power in the odd (upper set of curves) and even (lower set of curves) cores of NEMO fibers with two, four, and eight cores as a function of propagation distance, for the same parameter values as in the star-point of Fig. 3. The calculation of the average power in each core is

[2]This can be seen in a simple way for short propagation distance by analogy with the case of non-degenerate mode groups [29] or weakly coupled MCFs [30].

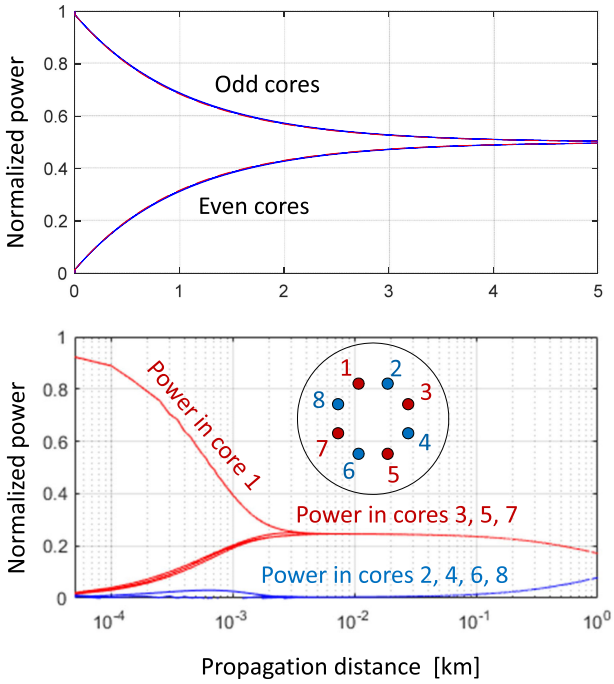

Fig. 5. The solid curves in the top panel show the total power in the odd (upper set of curves) and even (lower set of curves) cores as a function of propagation distance for NEMO fibers with four, six, and eight cores, observed by exciting a single polarization of the first core at the fiber input. The dashed curves refer to a two-core fiber with the same parameter values and with a coupling coefficient greater by a factor of $\sqrt{2}$. The fiber and perturbation parameters correspond to the star point in Fig. 3. The bottom panel shows the evolution of the optical power in the individual cores of the 8-core NEMO fiber, for the same input excitation used in the top panel.

detailed in Sec. IV, while the numerical values of all of the parameters are provided in Sec. V. The curves describe the average-power evolution seen when only the x-polarization of the first core is excited at the fiber input. The dashed curves represent the average powers in the two cores of a two-core NEMO fiber with the same parameters of the fibers with larger core counts, except that the inter-core distance was reduced so as to increase the coupling coefficient by a factor of $\sqrt{2}$. The perfect overlap between all curves proves the scaling argument discussed above. In the bottom panel of the same figure we show the evolution of the optical power in each of the cores of the 8-core NEMO fiber. The plot shows that the power transient is the same in all of the cores belonging to the same group, as if they were all directly coupled to each other, rather than through their nearest neighbors. This result is a manifestation of the tunneling-equivalent mentioned above.

B. Accounting for Effective-Refractive Index Fluctuations

The results shown in Figs. 1 and 3 were obtained by accounting only for random polarization-mode coupling in the each core. Another important source of randomness in the field propagation is represented by the fluctuations of the effective refractive indexes of the individual cores. These fluctuations can be included in the model, as described in Section III-B. In Fig. 6 we plot the MD coefficient for the same four-core NEMO fibers of Fig. 3, where we included random fluctuations of the effective

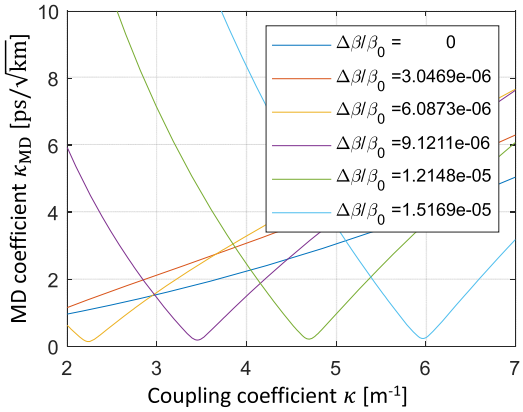

Fig. 6. Modal dispersion coefficient versus coupling coefficient for the same four-core NEMO fiber of Fig. 3, where effective-refractive index random fluctuations in the individual cores are added to the intra-core random polarization coupling.

refractive indexes of each core. These fluctuations are modeled as independent Gaussian processes with a root-mean square value of $\Delta n_{\rm rms}$ such that $\omega \Delta n_{\rm rms}/c = \Delta\beta/20$, and a two-sided exponential correlation function with the same correlation length of the cores birefringence $L_C = 0.1$ m, namely

$$\langle \Delta n_i(z') \Delta n_i(z'') \rangle = \Delta n_{\rm rms}^2 e^{-\frac{|z'-z''|}{L_C}}. \tag{17}$$

The comparison with Fig. 3 shows that the effect of the refractive-index fluctuations is to reduce the steepness of the individual curves (thereby reducing the sensitiveness of $\kappa_{\rm MD}$ to κ), while leaving the optimal core spacing values unchanged. The minimum value of $\kappa_{\rm MD}$ also reduces as a consequence of the effective-index fluctuations (this reduction is larger as $\Delta n_{\rm rms}$ increases).

III. Theory

The quantitative characterization of MD relies on the notion of the intensity impulse response (IIR), a fiber property that can be conveniently measured in experiments. The IIR, which we denote as $r(t)$ [23], is defined through the relation

$$I(t) = \int_{-\infty}^{+\infty} r(t-t') |\psi_0(t')|^2 {\rm d}t, \tag{18}$$

were $I(t)$ is the output optical power that is measured by transmitting a polarized signal waveform $\psi_0(t)$ in any one of the fiber cores. In practice the same waveform is transmitted in two orthogonal polarizations of each core and $I(t)$ is obtained by averaging the corresponding output intensity waveforms. Equation (18) holds in the regime of strong random mixing between cores, and it requires that the bandwidth of the input waveform be significantly larger than the modal dispersion bandwidth [23]. Under these circumstances, the IIR is Gaussian-shaped [9], [23], [31],

$$r(t) = \frac{1}{\sqrt{2\pi T^2}} e^{-\frac{t^2}{2T^2}}, \tag{19}$$

where T is what we refer to as its duration. Our analysis is based on the relation between T and the modal dispersion vector $\vec{\tau}$ [17],

[23],

$$T^2 = \frac{\langle \tau^2 \rangle}{4\,N^2}, \tag{20}$$

where $\tau^2 = \vec{\tau}\cdot\vec{\tau}$, which leaves us with the task of evaluating the ensemble average $\langle \tau^2 \rangle$. To this end, we recall that the generalized Jones vector $\vec{E}$, which is obtained by stacking the Jones vectors $\vec{E}_k$ describing the electric field in the individual cores on top of one another, obeys the following evolution equation,

$$\frac{\partial \vec{E}}{\partial z} = i\mathbf{B}\vec{E}, \tag{21}$$

where $\mathbf{B}$ is a $2\,N \times 2\,N$ matrix, which can be expressed as

$$\mathbf{B} = \beta_c \mathbf{I} + \frac{\vec{b}\cdot\vec{\Lambda}}{2\,N} + \frac{\vec{n}\cdot\vec{\Lambda}}{2\,N}. \tag{22}$$

Here β_c is the (immaterial) core-averaged propagation constant, $\vec{\Lambda}$ is a vector whose $D = 4\,N^2 - 1$ components are the generalized $2N \times 2\,N$ Pauli matrices Λ_j, and $\vec{b}$ and $\vec{n}$ are generalized birefringence vectors accounting for the deterministic fiber characteristics and for the perturbations, respectively. The D components of $\vec{b}$ and $\vec{n}$ can be extracted as $b_j = \mathrm{trace}[\Lambda_j(\vec{b}\cdot\vec{\Lambda})]/2\,N$ and $n_j = \mathrm{trace}[\Lambda_j(\vec{n}\cdot\vec{\Lambda})]/2\,N$ [9].

For a two-core fiber, assuming that the perturbations result in intra-core polarization-mode coupling only, one can find

$$\frac{\vec{b}\cdot\vec{\Lambda}}{2\,N} = \begin{bmatrix} -\frac{\Delta\beta}{2}\mathbf{I} & \kappa\mathbf{I} \\ \kappa\mathbf{I} & \frac{\Delta\beta}{2}\mathbf{I} \end{bmatrix} \tag{23}$$

$$\frac{\vec{n}\cdot\vec{\Lambda}}{2\,N} = \begin{bmatrix} \frac{\vec{\beta}_1\cdot\vec{\sigma}}{2} & 0 \\ 0 & \frac{\vec{\beta}_2\cdot\vec{\sigma}}{2} \end{bmatrix}, \tag{24}$$

with $N = 2$, $\vec{b} = 2\sqrt{2}\kappa(\hat{e}_7 + \hat{e}_{13}) + 2\Delta\beta\hat{e}_{15}$, and $\vec{n} = \sqrt{2}(\beta_{1,1}\hat{e}_1 + \beta_{1,2}\hat{e}_2 + \beta_{1,3}\hat{e}_3 + \beta_{2,1}\hat{e}_4 + \beta_{2,2}\hat{e}_5 + \beta_{2,3}\hat{e}_6)$. Note that the vector $\vec{b}$ can therefore be expressed as

$$\vec{b} = N(2\kappa\hat{b}_1 + \Delta\beta\hat{b}_2) \tag{25}$$

with $\hat{b}_1 \cdot \hat{b}_2 = 0$. For the four-core NEMO fiber, the above matrices change into

$$\frac{\vec{b}\cdot\vec{\Lambda}}{2\,N} = \begin{bmatrix} -\frac{\Delta\beta}{2}\mathbf{I} & \kappa\mathbf{I} & 0 & \kappa\mathbf{I} \\ \kappa\mathbf{I} & \frac{\Delta\beta}{2}\mathbf{I} & \kappa\mathbf{I} & 0 \\ 0 & \kappa\mathbf{I} & -\frac{\Delta\beta}{2}\mathbf{I} & \kappa\mathbf{I} \\ \kappa\mathbf{I} & 0 & \kappa\mathbf{I} & \frac{\Delta\beta}{2}\mathbf{I} \end{bmatrix} \tag{26}$$

$$\frac{\vec{n}\cdot\vec{\Lambda}}{2\,N} = \begin{bmatrix} \frac{\vec{\beta}_1\cdot\vec{\sigma}}{2}\mathbf{I} & 0 & 0 & 0 \\ 0 & \frac{\vec{\beta}_2\cdot\vec{\sigma}}{2}\mathbf{I} & 0 & 0 \\ 0 & 0 & \frac{\vec{\beta}_3\cdot\vec{\sigma}}{2}\mathbf{I} & 0 \\ 0 & 0 & 0 & \frac{\vec{\beta}_4\cdot\vec{\sigma}}{2}\mathbf{I} \end{bmatrix}, \tag{27}$$

with $\vec{b} = 2\sqrt{2}\kappa\sqrt{2}(\hat{e}_{13} + \hat{e}_{19} + \hat{e}_{29} + \hat{e}_{35} + \hat{e}_{37} + \hat{e}_{43} + \hat{e}_{53} + \hat{e}_{59}) + \Delta\beta(-2\sqrt{2}\hat{e}_{61} + 4\hat{e}_{62}/\sqrt{6} - 4\hat{e}_{63}/\sqrt{3})$, and $\vec{n} = \sqrt{4}(\beta_{1,1}\hat{e}_1 + \beta_{1,2}\hat{e}_2 + \beta_{1,3}\hat{e}_3 + \beta_{2,1}\hat{e}_4 + \beta_{2,2}\hat{e}_5 + \beta_{2,3}\hat{e}_6 + \beta_{3,1}\hat{e}_7 + \beta_{3,2}\hat{e}_8 + \beta_{3,3}\hat{e}_9 + \beta_{4,1}\hat{e}_{10} + \beta_{4,2}\hat{e}_{11} + \beta_{4,3}\hat{e}_{12})$, or equivalently

$$\vec{b} = N(2\sqrt{2}\kappa\hat{b}_1 + \Delta\beta\hat{b}_2), \tag{28}$$

again with $\hat{b}_1 \cdot \hat{b}_2 = 0$ (notice that by the same symbols $\hat{b}_1$ and $\hat{b}_2$ we are denoting different vectors in Eqs. (25) and (28)). The form of $\vec{b}$ does not change from four to larger core counts, while it differs by the same factor of $\sqrt{2}$ in front of κ with respect to the case of the two-core fiber Eq. (25). This difference explains the scaling factor of $\sqrt{2}$ in the expression of $\vec{b}\cdot\vec{b}_\omega$ discussed in Sec. II-A.

The MD vector $\vec{\tau}$ evolves with propagation distance according to the equation [17]

$$\frac{\partial \vec{\tau}}{\partial z} = \vec{b}_\omega + (\vec{b} + \vec{n}) \times \vec{\tau}, \tag{29}$$

where by the symbol $\times$ we denote the generalized vector product [9]. The evolution equation for τ^2, reads as

$$\frac{\partial \tau^2}{\partial z} = 2\vec{\tau}\cdot\frac{\partial \vec{\tau}}{\partial z} = 2\vec{b}_\omega\cdot\vec{\tau}, \tag{30}$$

which, for the purpose of evaluating $\langle \tau^2 \rangle$, leaves us with the evaluation of $\langle \vec{\tau} \rangle$. To this end we express Eq. (29) in a rotating reference frame that maps $\vec{\tau}$ into $\tilde{\vec{\tau}} = \exp(-z\vec{b}\times)\vec{\tau}$ (and similarly $\vec{b}_\omega$ and $\vec{n}$ into $\tilde{\vec{b}}_\omega$ and $\tilde{\vec{n}}$, respectively), with the result

$$\frac{\partial \tilde{\vec{\tau}}}{\partial z} = \tilde{\vec{b}}_\omega + \tilde{\vec{n}} \times \tilde{\vec{\tau}}. \tag{31}$$

We then integrate (31) over the interval Δz, which yields

$$\Delta\tilde{\vec{\tau}} = \int_{\Delta z} \mathrm{d}z' \tilde{\vec{b}}_\omega(z') + \int_{\Delta z} \mathrm{d}z' \tilde{\vec{n}}(z') \times \tilde{\vec{\tau}}(z'), \tag{32}$$

where $\Delta\tilde{\vec{\tau}} = \tilde{\vec{\tau}}(z + \Delta z) - \tilde{\vec{\tau}}(z)$, and, reiterating this procedure,

$$\begin{aligned} \Delta\tilde{\vec{\tau}} = &\int_z^{z+\Delta z} \mathrm{d}z' \tilde{\vec{b}}_\omega(z') + \int_z^{z+\Delta z} \mathrm{d}z' \tilde{\vec{n}}(z') \times \tilde{\vec{\tau}}(z) \\ &+ \int_z^{z+\Delta z} \mathrm{d}z' \int_z^{z'} \mathrm{d}z'' \tilde{\vec{n}}(z') \times \tilde{\vec{b}}_\omega(z'') \\ &+ \int_z^{z+\Delta z} \mathrm{d}z' \int_z^{z'} \mathrm{d}z'' \tilde{\vec{n}}(z') \times \tilde{\vec{n}}(z'') \times \tilde{\vec{\tau}}(z'). \end{aligned} \tag{33}$$

For a proper choice[3] of Δz, the third term on the right-hand side of the equality is higher-order than Δz and therefore can be neglected, while in the fourth term $\tilde{\vec{\tau}}(z')$ can be replaced with $\tilde{\vec{\tau}}(z)$ and the remaining double integral with its ensemble average, extending the inner integral to infinity. This procedure yields the following evolution equation for $\Delta\tilde{\vec{\tau}}$ that can be interpreted in the Ito sense,

$$\Delta\tilde{\vec{\tau}} = \mathbf{A}\vec{b}_\omega\Delta z + \Delta\vec{W} \times \tilde{\vec{\tau}} + \mathbf{Q}\tilde{\vec{\tau}}\Delta z, \tag{34}$$

where we defined

$$\Delta\vec{W} = \int_z^{z+\Delta z} \tilde{\vec{n}}(z')\mathrm{d}z' \tag{35}$$

$$\mathbf{A} = \frac{1}{\Delta z}\int_{\Delta z} e^{-z'\vec{b}\times}\mathrm{d}z' \tag{36}$$

[3] As discussed in [17], the perturbations must be small enough so as to produce small changes of the MD vector $\tilde{\vec{\tau}}$ in the interval Δz. On the other hand, Δz must be much greater than the correlation length L_C.

$$\mathbf{Q} = \frac{1}{\Delta z}\int_{\Delta z} e^{z'\vec{b}\times}\mathbf{q}e^{-z'\vec{b}\times}\mathrm{d}z' \tag{37}$$

with

$$\mathbf{q} = \sum_{i,j=1}^{D}\hat{e}_i \times \left[\int_0^\infty \mathrm{N}_{i,j}(\zeta)e^{\zeta\vec{b}\times}\mathrm{d}\zeta\hat{e}_j\right]\times, \tag{38}$$

and $\mathrm{N}_{i,j}(z'-z'') = \langle n_i(z')n_j(z'')\rangle$. Here by the symbol $\hat{u}\times$ we denote a matrix such that $(\hat{u}\times)\vec{v}$ equals the generalized vector product $\hat{u}\times\vec{v}$. We note that the integration with respect to z' in the definition of $\mathbf{A}$ averages out the fast rotations produced by $\exp(z'\vec{b}\times)$, and therefore the effect of applying $\mathbf{A}$ to a vector is to perform a projection of that vector onto the subspace of the eigenstates of $\vec{b}\times$. Similar considerations apply to how the matrix $\mathbf{Q}$ can be extracted from the matrix $\mathbf{q}$. A procedure for extracting the numerical values of $\mathbf{A}$ and $\mathbf{Q}$ is described in the appendix.

By taking the ensemble average of both sides of Eq. (34), and using the fact that within the described assumptions $\Delta\vec{W}$ is zero-mean and independent of $\tilde{\vec{\tau}}$, one finds the following equation for $\langle\tilde{\vec{\tau}}\rangle$,

$$\frac{\partial\langle\tilde{\vec{\tau}}\rangle}{\partial z} = \mathbf{A}\vec{b}_\omega + \mathbf{Q}\tilde{\vec{\tau}}, \tag{39}$$

whose solution, in the original reference frame, is

$$\langle\vec{\tau}\rangle = e^{z\vec{b}\times}\mathbf{Q}^{-1}\left(e^{\mathbf{Q}z}-\mathbf{I}\right)\mathbf{A}\vec{b}_\omega, \tag{40}$$

and hence, using Eq. (30),

$$\langle\tau^2\rangle = 2\vec{b}_\omega\cdot\int_0^z e^{z'\vec{b}\times}\mathbf{Q}^{-1}\left(e^{\mathbf{Q}z'}-\mathbf{I}\right)\mathbf{A}\vec{b}_\omega\mathrm{d}z'. \tag{41}$$

The above can be simplified by noting that integration with respect to z' averages out the fast rotations produced by $\exp(z'\vec{b}\times)$. This is equivalent to applying $\mathbf{A}$ to $\vec{b}_\omega$, with the result

$$\langle\tau^2\rangle = 2(\mathbf{A}\vec{b}_\omega)\cdot\mathbf{Q}^{-1}\left[\mathbf{Q}^{-1}\left(e^{\mathbf{Q}z}-\mathbf{I}\right)-\mathbf{I}z\right]\mathbf{A}\vec{b}_\omega. \tag{42}$$

The delay spread $T^2 = \langle\tau^2\rangle/4\,N^2$ is then obtained in the form

$$\begin{aligned} T^2 &= \frac{2}{4\,N^2}(\mathbf{A}\vec{b}_\omega)\cdot\mathbf{Q}^{-1}\left[\mathbf{Q}^{-1}\left(e^{\mathbf{Q}z}-\mathbf{I}\right)-\mathbf{I}z\right]\mathbf{A}\vec{b}_\omega \\ &\simeq \kappa_{\mathrm{MD}}^2 z, \end{aligned} \tag{43}$$

where the second equality holds asymptotically for large values of z, with

$$\kappa_{\mathrm{MD}} = \frac{\sqrt{-2(\mathbf{A}\vec{b}_\omega)\cdot\mathbf{Q}^{-1}(\mathbf{A}\vec{b}_\omega)}}{2\,N}. \tag{44}$$

Notice that Eq. (44) differs from Eq. (4) of [17] by the presence of the matrix $\mathbf{A}$. In the case of homogeneous-core MCFs, where $\vec{b}$ is parallel to $\vec{b}_\omega$ as assumed in [17], the product $\mathbf{A}\vec{b}_\omega$ reduces to $\vec{b}_\omega$, and therefore $\mathbf{A}$ reduces to the identity matrix.

In the remainder of this section we specialize the expression of $\mathbf{q}$ to the cases considered in the figures of in Sect. II.

A. Intra-Core Random Polarization-Mode Coupling

Figs. 1, 3, and 5 have been obtained assuming identically distributed and statistically independent random birefringence processes in the individual cores, in which case only the first $3\,N$ components of $\vec{n}$ are non-zero. In particular, using the generalization of Eq. (27) to the case of N cores jointly with (8), one finds

$$\langle n_i(z')n_j(z'')\rangle = \delta_{ij}\frac{N}{3}\left(\frac{2\pi}{L_B}\right)^2 e^{-\frac{|z'-z''|}{L_C}},\ (i,j)\le 3\,N \tag{45}$$

where δ_{ij} is the Kronecker delta, which gives $\mathbf{q}$ in the following form

$$\mathbf{q} = \frac{N}{3}\left(\frac{2\pi}{L_B}\right)^2 L_C\sum_{i=1}^{3N}\hat{e}_i\times\left[\left(\mathbf{I}-L_C\vec{b}\times\right)^{-1}\hat{e}_i\right]\times. \tag{46}$$

Equation (46) determines the dependence of MD on the beat length and correlation length. In particular, on the one hand it shows that (in the absence of perturbations other than random polarization-mode coupling) the MD coefficient is proportional to L_B. On the other hand, it suggests that the dependence on L_C is less obvious. We found that for the numerical values of the parameters assumed in this work, increasing L_C results in a reduction of the MD coefficient around the optimal core pitch and in an increase elsewhere.

B. Effective-Index Random Fluctuations

Fluctuations of the effective index in the individual cores translate in non-zero values of the last $N-1$ components of $\vec{n}$ [9]. We assume that they are statistically uncorrelated with polarization-mode coupling and denote the deviation of the effective index of core i from its nominal value by Δn_i. In the case of a two-core fibers, they contribute to the field propagation matrix with the term

$$\frac{\vec{n}\cdot\vec{\Lambda}}{2\,N} = \frac{\omega}{c}\begin{bmatrix}\Delta n_1\mathbf{I} & 0\\ 0 & \Delta n_2\mathbf{I}\end{bmatrix}, \tag{47}$$

from which one can extract

$$\vec{n} = 2\frac{\omega}{c}(\Delta n_1-\Delta n_2)\hat{e}_{15}. \tag{48}$$

For identically distributed independent zero-mean deviations with correlation function Eq. (17), the above yields

$$\mathbf{q} = 8\frac{\omega^2}{c^2}\Delta n_{\mathrm{rms}}^2 L_C\hat{e}_{15}\times\left[\left(\mathbf{I}-L_C\vec{b}\times\right)^{-1}\hat{e}_{15}\right]\times. \tag{49}$$

In the case of N cores, the expression for $\vec{n}$ becomes

$$\vec{n} = \sum_{j=D-N+2}^{D}\sqrt{\frac{N}{j^2+j}}\frac{\omega}{c}\left(\sum_{k=1}^{j}2\Delta n_k - 2j\Delta n_{j+1}\right)\hat{e}_j \tag{50}$$

and for identically distributed independent zero-mean deviations, this yields

$$\langle n_i(z')n_j(z'')\rangle = 4\,N\frac{\omega^2}{c^2}\delta_{ij}\langle\Delta n(z')\Delta n(z'')\rangle, \tag{51}$$

with $(i,j) = (D-N+2)\cdots D$, and hence

$$\mathbf{q} = 4N\frac{\omega^2}{c^2}\Delta n_{\mathrm{rms}}^2 \; L_C \sum_{i=D-N+2}^{D} \hat{e}_i \times \left[\left(\mathbf{I} - L_C\vec{b}\times\right)^{-1}\hat{e}_i\right]\times . \tag{52}$$

The results shown in Fig. 6 were obtained by computing $\mathbf{q}$ as a sum of the expressions in (46) and (52).

IV. Spatial Dynamics of Random Mode Mixing

In this section we characterize the space dynamics of random mode mixing. Knowledge of the length-scale on which full random mixing is achieved is key to assess the effectiveness with which nonlinear distortions are mitigated. In fact, the suppression of nonlinear distortions requires that random mode mixing occurs on a length-scale much shorter than the relevant nonlinear length-scale (which can be quantified in terms of nonlinear pulse collisions when the transmission of pulse-code modulated signals is considered [32]).

The length-scale of random coupling can be characterized by looking at the evolution of the average field power in the fiber cores. To this end we consider the matrix $\mathbf{P} = \langle\vec{E}\vec{E}^{\dagger}\rangle$, so that the average power in the n-th core is given by $P_{2n-1,2n-1} + P_{2n,2n}$ (the two terms account for the average power in two orthogonal polarizations), with $n = 1\cdots N$. Using the Stokes-space formalism [9], $\mathbf{P}$ can be expressed as

$$\mathbf{P} = \langle\vec{E}\vec{E}^{\dagger}\rangle = \frac{1}{2\,N}\left(\mathbf{I} + \langle\vec{s}\rangle\cdot\vec{\Lambda}\right), \tag{53}$$

where $\vec{s}$ is the generalized Stokes vector associated to the generalized Jones vector $\vec{E}$, and therefore the problem of finding $\mathbf{P}$ reduces to the evaluation of $\langle\vec{s}\rangle$. Notice that when $\langle\vec{s}\rangle$ vanishes only the diagonal terms of $\mathbf{P}$ are non-zero and they are all equal to $1/2\,N$, indicating that the transmitted power is equalized among all the space- and polarization- modes. In order to evaluate $\langle\vec{s}\rangle$ we use the evolution equation for $\vec{s}$ [9],

$$\frac{\mathrm{d}\vec{s}}{\mathrm{d}z} = \left(\vec{b} + \vec{n}\right)\times\vec{s} \tag{54}$$

which in the rotating reference frame changes into

$$\frac{\mathrm{d}\tilde{\vec{s}}}{\mathrm{d}z} = \tilde{\vec{n}}\times\tilde{\vec{s}}. \tag{55}$$

Following a procedure similar to the one adopted for the derivation of $\langle\vec{\tau}\rangle$, we integrate the latter over Δz,

$$\Delta\tilde{\vec{s}} = \int_z^{z+\Delta z}\tilde{\vec{n}}(z')\times\tilde{\vec{s}}(z')\mathrm{d}z,' \tag{56}$$

then iterate the integration,

$$\Delta\tilde{\vec{s}} = \left[\int_z^{z+\Delta z}\tilde{\vec{n}}(z')\mathrm{d}z'\right]\times\tilde{\vec{s}}(z) + \int_z^{z+\Delta z}\int_z^{z+\Delta z}\tilde{\vec{n}}(z')\times\tilde{\vec{n}}(z'')\times\tilde{\vec{s}}(z'')\mathrm{d}z''\mathrm{d}z,' \tag{57}$$

replace $\tilde{\vec{s}}(z'')$ with $\tilde{\vec{s}}(z)$, and the double integral with its average, with the result

$$\Delta\tilde{\vec{s}} = \Delta\vec{W}(z)\times\tilde{\vec{s}}(z) + \mathbf{Q}\tilde{\vec{s}}(z)\Delta z \tag{58}$$

After taking the average on both sides of the equation, we obtain

$$\Delta\langle\tilde{\vec{s}}\rangle = \mathbf{Q}\langle\tilde{\vec{s}}(z)\rangle\Delta z, \tag{59}$$

which yields

$$\langle\tilde{\vec{s}}(z)\rangle = \exp\{\mathbf{Q}z\}\tilde{\vec{s}}(0), \tag{60}$$

and returning to the original reference frame,

$$\langle\vec{s}(z)\rangle = \exp\{z\vec{b}\times\}\exp\{\mathbf{Q}z\}\vec{s}(0). \tag{61}$$

This result, compared to Eq. (44), shows that the matrix $\mathbf{Q}$ plays opposing roles in the reduction of modal dispersion and in the acceleration of random mode mixing, and therefore it entails a trade-off in the simultaneous pursuit of two objectives. The distance at which full mixing is achieved is characterized by the eigenvalue of Q with the smallest absolute-real part, which sets the distance at which $\langle\vec{s}(z)\rangle$ is suppressed, and hence the optical power is equalized on average among all modes.

V. Numerical Results

In this section we expand on the numerical results presented in the previous sections and provide the main details that are necessary for the numerical evaluation of the theoretical expressions involved.

We consider a step-index refractive index profile, where the frequency-dependence of the core index is given by a Sellmeier third-order formula

$$n_1^2(\lambda) = 1 + \sum_{k=1}^{3} N_k\frac{\lambda^2}{\lambda^2 - \lambda_k^2}, \tag{62}$$

with $\lambda = 2\pi c/\omega$. We assume the same frequency dependence for the cladding refractive index, which therefore differs from the core index by a constant value Δn. In this study we assume a relative index difference of 0.39% at $\lambda_0 = 1550$ nm and the following Sellmeier coefficient: $N_1 = 0.6961663; \lambda_1 = 0.0684043\,\mu\mathrm{m}; N_2 = 0.4079426; \lambda_2 = 0.1162414\,\mu\mathrm{m}; N_3 = 0.8974794; \lambda_3 = 9.896161\,\mu\mathrm{m}$.

The propagation constant β is obtained by solving the familiar characteristic equation $xJ_1(x)/J_0(x) = \sqrt{V^2-x^2}K_1(\sqrt{V^2-x^2})/K_0(\sqrt{V^2-x^2})$, where $x^2 = r^2(n_1^2\omega^2/c^2 - \beta^2)$ and where $V = 2\pi r\sqrt{n_1^2 - n_2^2}/\lambda$ is the normalized frequency, with r denoting the core radius. By J_n and K_n we denote Bessel functions of the first kind and modified Bessel functions of the second kind, respectively. The reference propagation constant β_0 corresponds to a core radius $r_0 = 4.6\,\mu\mathrm{m}$ at λ_0, and the values of $\Delta\beta = \beta(r) - \beta(r_0)$ are obtained by increasing the core radius r from r_0 to $r_0 + 0.03\,\mu\mathrm{m}$. The frequency derivative $\Delta\beta_\omega = \beta_\omega(r) - \beta_\omega(r_0)$ results from analytically differentiating the characteristic equation with respect to ω.

The expression for the deterministic coupling coefficient follows from couple-mode theory under the

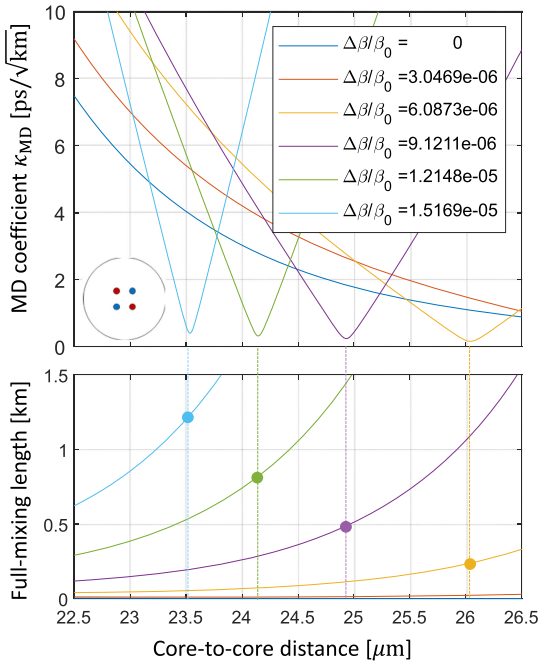

Fig. 7. The top panel shows a plot of the MD coefficient versus the core-to-core distance in four-core NEMO fibers with the displayed values of the propagation-constant mismatch. The bottom panel is a plot of the corresponding full-mixing length.

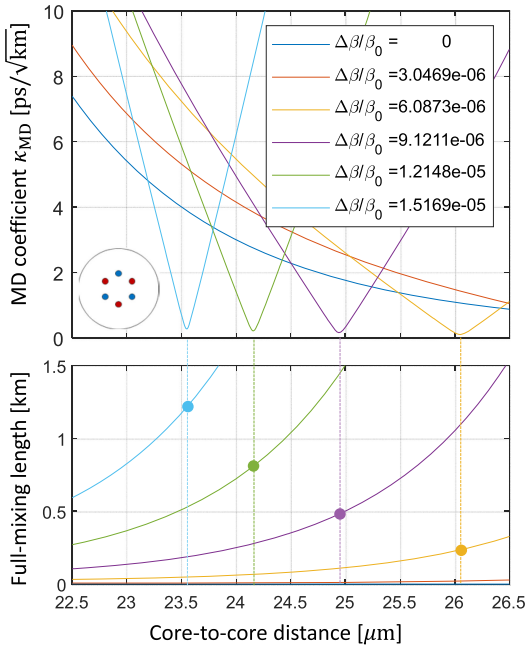

Fig. 8. Same as in Fig. 7 for a six-core NEMO fiber.

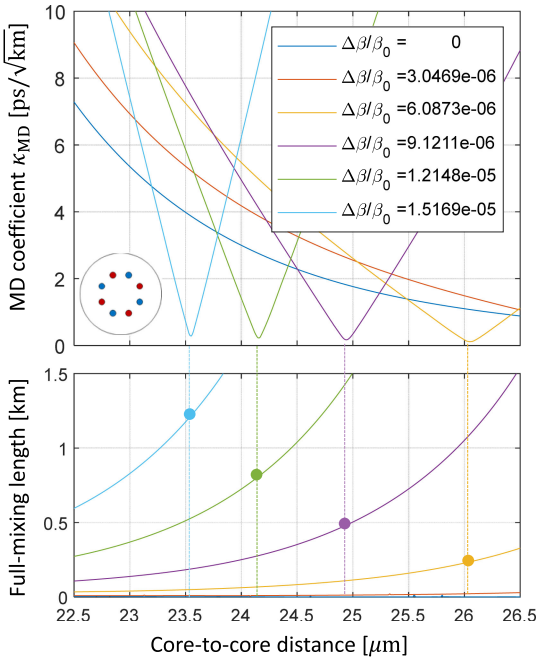

Fig. 9. Same as in Fig. 7 for an eight-core NEMO fiber.

assumption of nearly identical cores [18], and using the reference core radius r_0 in all cases. That is, $\kappa = \sqrt{1-n_2^2/n_1^2}\, x_0^2\, V^{-3} r_0^{-1} K_0(\sqrt{V^2-x_0^2}\, d/r_0) / K_1^2(\sqrt{V^2-x_0^2})$, where x_0 is the solution to the characteristic equation for the reference core radius r_0, and d is the varying distance between neighboring cores. The frequency derivative of κ is also obtained by analytically differentiating the expression given above. Notice that, given the small range in which the core radius is varied to produce $\Delta\beta$, the use of r_0 in the expressions of κ and κ_ω does not compromise the accuracy with which these two parameters are evaluated. In addition, we note that the off-diagonal elements of the matrix accounting for the non-orthogonality of the local modes (i.e. the overlap integrals between the fundamental mode profiles of the individual cores) [27] are at most of the order of 10^{-4} to 10^{-3} in the range of core-to-core distance values considered in this work. Inversion of this matrix produces (beyond a negligible change in the coupling coefficients between nearest-neighboring cores) coupling between second-neighboring cores with coupling coefficients that are smaller than κ by the same order of magnitude. For this reason we neglect them with no loss of accuracy. Neglecting these coefficients is indeed consistent with the original assumption of negligible overlap between the modes of cores that are not nearest neighbors.

In Fig. 7 we consider a four-core NEMO fiber. In the top panel we plot the MD coefficient of Eq. (44) as a function of the core-to-core distance d for the displayed values of $\Delta\beta/\beta_0$, taking into account intra-core random polarization coupling only. The matrix $\mathbf{Q}$ is computed using the expression in Eq. (52) for $\mathbf{q}$. In the bottom panel we plot the full-mixing length $\ell_{\rm fm}$, which, denoting by $-1/\ell_n + i\phi_n$ the n-th eigenvalue of $\mathbf{Q}$, is defined as the largest value of ℓ_n (with respect to $n = 1 \cdots D$). The plot shows that introducing some inhomogeneity between cores increases the full-mixing length, as expected, thereby reducing the mode mixing efficiency. We note, however, that the increased full-mixing length is of the order of a few hundreds of meters – significantly shorter than the length-scale of nonlinear effects that are responsible for nonlinear signal distortions. Therefore the known advantage of strong mode coupling in terms of tolerance to nonlinear distortions is not compromised.

The quantities plotted in Figs. 8 and 9 are the same as in Fig. 7, except that they refer to six- and eighth-core NEMO fibers. Like

for Fig. 7, the curves in the top and bottom panels of Figs. 8 and 9 are also plotted in Fig. (3), yet versus the coupling coefficient κ.

We conclude this section by noting that the optimization of the MD coefficient requires accurate control on the core pitch, as indicated by the steep dependence of $\kappa_{\rm MD}$. This steepness reduces for smaller values of $\Delta\beta$, but in that case the accuracy required in the control of the core sizes increases. We stress, however, that this requirement may be relaxed, for instance by accounting for propagation effects other than intra-core random polarization-mode coupling, as noted in the context of Fig. 6.

VI. Simulations

In this section we validate the theoretical results presented in Sects. II and V by comparison with Monte-Carlo simulations.

We modeled the fiber as a concatenation of wave-plates of length Δz, so that, considering for illustration purposes the four-core fiber, propagation of the generalized Jones vector through the h-th section was described by the matrix

$$\mathbf{U}_h = \exp\left[i \begin{pmatrix} \frac{\vec{\beta}_{1,h}\cdot\vec{\sigma}}{2} & \kappa\mathbf{I} & \mathbf{0} & \kappa\mathbf{I} \\ \kappa\mathbf{I} & \frac{\vec{\beta}_{2,h}\cdot\vec{\sigma}}{2} & \kappa\mathbf{I} & 0 \\ 0 & \kappa\mathbf{I} & \frac{\vec{\beta}_{3,h}\cdot\vec{\sigma}}{2} & \kappa\mathbf{I} \\ \kappa\mathbf{I} & 0 & \kappa\mathbf{I} & \frac{\vec{\beta}_{4,h}\cdot\vec{\sigma}}{2} \end{pmatrix} \Delta z \right], \quad (63)$$

where $\vec{\beta}_{n,h}$ is the birefringence vector of core n. The step size was set to be significantly smaller than the birefringence correlation length, so that the birefringence vector could be safely assumed to be constant within each step. In particular we sampled the underlying Ornstein-Uhlenbeck processes with a spacing of $L_C/15$. The Ornstein-Uhlenbeck processes were generated with a resolution ten times greater by numerically filtering spatially white Gaussian noise,

$$\beta(z_k) = \frac{2\pi}{L_B}\sqrt{\frac{2}{L_C}}\int_{-\infty}^{z_k} e^{-\frac{z_k - z'}{L_C}}\,\mathrm{d}N(z'), \quad (64)$$

with $\langle N(z')N(z'')\rangle = \delta(z'-z'')$, and where we dropped the subscripts for ease of notation.

The accumulation of the MD vector was evaluated numerically using the concatenation rule for the matrix $\vec{\tau}\cdot\vec{\Lambda}$ [9], which reads as

$$\vec{\tau}(z_{h+1})\cdot\vec{\Lambda} = (\vec{b}_\omega\cdot\vec{\Lambda})\Delta z + \mathbf{U}_h[\vec{\tau}(z_h)\cdot\vec{\Lambda}]\mathbf{U}_h^\dagger. \quad (65)$$

The square MD vector length was extracted as $\tau^2(z_h) = \mathrm{Trace}\{[\vec{\tau}(z_h)\cdot\vec{\Lambda}]^2\}/2\,N$, and the ensemble average was performed using 1000 instantiations of the intra-core birefringence vectors. In Fig. 10 we show the simulation results for the evolution of $T = \sqrt{\langle\tau^2(z)\rangle}/2\,N$, obtained as described above. All plots refer to the case $\Delta\beta/\beta_0 = 1.2148\times10^{-5}$ of Figs. 1 and 7–9, and to the displayed core pitch values (the ones in the middle column correspond to the MD minima). The thick curves show the simulation results, while the thin dashed curves are a plot of the full expression of T in Eq. (43). As is evident from the plots, the agreement between theory and simulations is excellent in all cases, except for the optimal core-pitch value of the two-core fiber, where the theory fails by predicting an intensity impulse response duration smaller by about a factor of twenty, corresponding to a theoretical MD coefficient of about 0.0027 ps/km$^{1/2}$ versus a simulation result of about 0.047 ps/km$^{1/2}$.

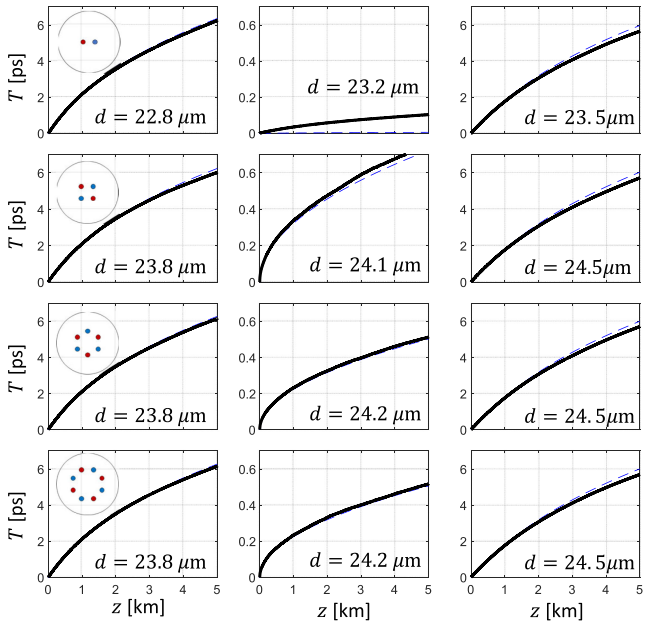

Fig. 10. Evolution of $T = \sqrt{\langle\tau^2(z)\rangle}/2\,N$ with respect to propagation distance. All panels refer to the case $\Delta\beta/\beta_0 = 1.2148\times10^{-5}$ of Figs. 1 and 7–9. Solid curves show the results of Monte-Carlo simulations, while dashed curves are the theoretical result.

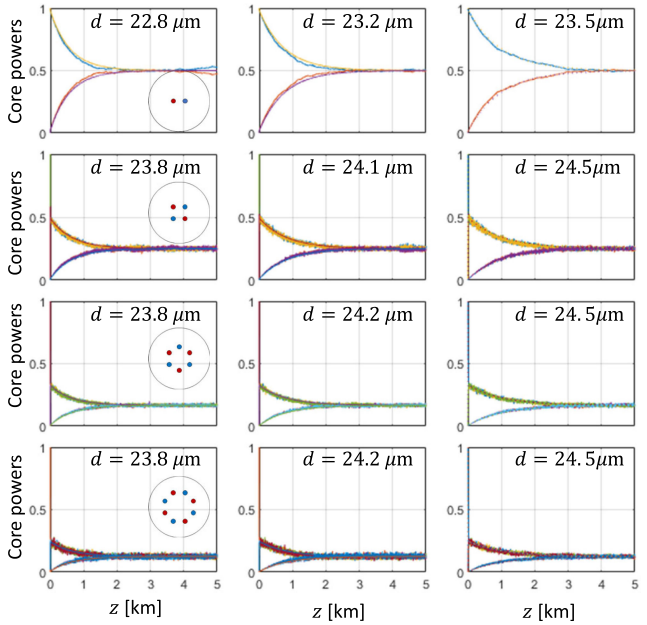

Fig. 11. Evolution of optical power with respect to propagation distance in the individual cores of NEMO fiber with two-to-eight cores. All panels refer to the case $\Delta\beta/\beta_0 = 1.2148\times10^{-5}$ of Figs. 1 and 7–9. Solid curves show the results of Monte-Carlo simulations, while dashed curves are the theoretical result.

In Fig. 11 we plot the average power in each core as a function of propagation distance, obtained by exciting only the x-polarization in the first core at the fiber input. The panels

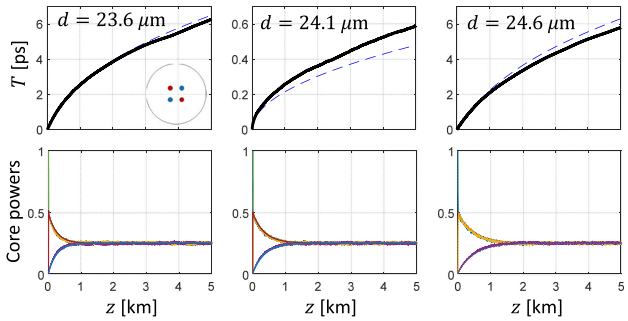

Fig. 12. Same as in Figs. 10 and 11 for a four-core NEMO fiber with independent random fluctuations of the effective refractive index in each core.

of Fig. 11 are in a one-to-one correspondence with those of Fig. 10. In the simulations, the optical power in each core was evaluated by summing the absolute-square values of the two components of the propagated field vector $\vec{E}(z_h)$ describing the excitations of the x and y polarizations in that core. In the cases of more than two cores, the power injected in the first core at the fiber input equalizes among all of the odd cores within a few meters (as seen in detail in the lower panel of Fig. 5), and then equalization among all of the cores is achieved on the full-mixing-length-scale ($\ell_{\rm fm}$, plotted in the bottom panels of Figs. 7–9).

In Fig. 12 we extend the simulation results of Figs. 10 and 11 in the case of the four-core NEMO fiber by including also random fluctuations of the effective refractive index in each core. In the simulations these were generated by sampling four independent Orstein-Uhlenbeck processes based on the expression

$$\Delta n(z_k) = \Delta n_{\rm rms}\sqrt{\frac{2}{L_C}}\int_{-\infty}^{z_k} e^{-\frac{z_k-z'}{L_C}}\,{\rm d}N(z'), \qquad (66)$$

with the same parameter settings used in Fig. 6.

VII. Conclusions

We proposed a design for coupled-core multi-core fibers that allows a substantial reduction of modal dispersion. In the proposed design an even number of cores are regularly distributed on a circle, so that each core is coupled to two identical cores with the same propagation-constant mismatch. The modal dispersion reduction follows from a proper balance between the frequency dependence of the propagation-constant mismatch and that of the inter-core coupling coefficient. We dub these fibers *NEar-zero MOdal-dispersion* (NEMO) fibers, and show that for up to eight cores the modeal dispersion coefficient can be reduced to values of the order of $0.1\ {\rm ps}/\sqrt{\rm km}$, typical for polarization-mode dispersion in legacy single-mode fibers.

Appendix
Numerical Extraction of $\mathbf{A}$ and $\mathbf{Q}$

The definition of matrices $\mathbf{A}$ and $\mathbf{Q}$ in Eqs. (36) and (37) relies on an interval Δz which is not specified quantitatively. In order to extract the numerical values of these two matrices, one can use the following procedure, which relies on the physical meaning of the integrals involved in Eqs. (36) and (37) – averaging out the fast-oscillating content of $\exp(-z\vec{b}\times)$ and $\exp(z\vec{b}\times)\mathbf{q}\exp(-z\vec{b}\times)$.

The first step is to numerically diagonalize the matrix $\vec{b}\times$ as $\vec{b}\times = \mathbf{C}{\rm Diag}\{i\lambda_1, i\lambda_2 \cdots i\lambda_D\}\mathbf{C}^{-1}$ and express $\exp(-z\vec{b}\times)$ as

$$\exp(-z\vec{b}\times) = \mathbf{C}\left(\sum_n e^{-i\lambda_n z}\mathbf{1}_{n,n}\right)\mathbf{C}^{-1}, \qquad (67)$$

where $\mathbf{1}_{n,n'}$ is a matrix whose (n,n') element is unit and all the others are zero.

For the extraction of $\mathbf{A}$ it is sufficient to replace the terms $\exp(-i\lambda_n z)$ for which $\lambda_n \neq 0$ with zero. These are the terms that would be averaged out by the integration over Δz.

For the extraction of $\mathbf{q}$, use of (67) yields

$$\exp(z\vec{b}\times)\mathbf{q}\exp(-z\vec{b}\times) = \mathbf{C}\left(\sum_{n,n'} q_{n,'n} e^{i(\lambda_n-\lambda_{n'})z}\mathbf{1}_{n,'n}\right)\mathbf{C}^{-1}. \qquad (68)$$

After the averaging the parenthesis on the right-hand side of the equality reduces to $\mathbf{q}$, where the terms $q_{n,'n}$ for which $\lambda_n \neq \lambda_{n'}$ are replaced with zero.

References

[1] T. Hayashi, *Multi-Core Fibers for Space Division Multiplexing*. Singapore: Springer Singapore, 2019, pp. 99–145. [Online]. Available: https://doi.org/10.1007/978-981-10-7087-7_66

[2] K.-P. Ho and J. M. Kahn, "Chapter 11 - Mode coupling and its impact on spatially multiplexed systems," *Optical Fiber Telecommunications (Sixth Edition)*, 6th ed., Ser. Optics and Photonics, I. P. Kaminow, T. Li, and A. E. Willner, Eds. Boston, MA, USA: Academic Press, 2013, pp. 491–568. [Online]. Available: https://www.sciencedirect.com/science/article/pii/B9780123969606000110

[3] R. Ryf and C. Antonelli, *Space-Division Multiplexing*. Cham: Springer, 2020, pp. 353–393. [Online]. Available: https://doi.org/10.1007/978-3-030-16250-4_10

[4] R. Ryf *et al.*, "Long-distance transmission over coupled-core multicore fiber," in *Proc. 42nd Eur. Conf. Opt. Commun. ECOC - Post Deadline Paper*, 2016, pp. 1–3.

[5] R. Ryf *et al.*, "Long-haul transmission over multi-core fibers with coupled cores," in *Proc. Eur. Conf. Opt. Commun.*, 2017, pp. 1–3.

[6] C. Antonelli, M. Shtaif, and A. Mecozzi, "Modeling of nonlinear propagation in space-division multiplexed fiber-optic transmission," *J. Lightw. Technol.*, vol. 34, no. 1, pp. 36–54, 2016.

[7] S. Mumtaz, R.-J. Essiambre, and G. P. Agrawal, "Reduction of nonlinear penalties due to linear coupling in multicore optical fibers," *IEEE Photon. Technol. Lett.*, vol. 24, no. 18, pp. 1574–1576, Sep. 2012.

[8] K.-P. Ho and J. M. Kahn, "Statistics of group delays in multimode fiber with strong mode coupling," *J. Lightw. Technol.*, vol. 29, no. 21, pp. 3119–3128, 2011.

[9] C. Antonelli, A. Mecozzi, M. Shtaif, and P. J. Winzer, "Stokes-space analysis of modal dispersion in fibers with multiple mode transmission," *Opt. Exp.*, vol. 20, no. 11, pp. 11718–11733, May 2012.

[10] T. Hayashi *et al.*, "Coupled-core multi-core fibers: High-spatial-density optical transmission fibers with low differential modal properties," in *Proc. Eur. Conf. Opt. Commun.*, 2015, pp. 1–3.

[11] Y. Yamada *et al.*, "Spatial mode dispersion control in a coupled MCF using high density cabling parameters," in *Proc. Opt. Fiber Commun. Conf. Exhib.*, 2020, pp. 1–3.

[12] T. Hayashi *et al.*, "Field-deployed multi-core fiber testbed," in *Proc. 24th OptoElectron. Commun. Conf. Int. Conf. Photon. Switching Comput.*, Jul. 2019, pp. 1–3.

[13] T. Sakamoto, T. Mori, M. Wada, T. Yamamoto, F. Yamamoto, and K. Nakajima, "Fiber twisting- and bending-induced adiabatic/nonadiabatic super-mode transition in coupled multicore fiber," *J. Lightw. Technol.*, vol. 34, no. 4, pp. 1228–1237, Feb. 2016.

[14] B. Huang *et al.*, "Minimizing the modal delay spread in coupled-core two-core fiber," in *Proc. Conf. Lasers Electro- Opt.*, 2016, pp. 1–2.
[15] T. Sakamoto, T. Mori, M. Wada, T. Yamamoto, F. Yamamoto, and K. Nakajima, "Strongly-coupled multi-core fiber and its optical characteristics for mimo transmission systems," *Opt. Fiber Technol.*, vol. 35, pp. 8–18, 2017.
[16] S. Arik and J. M. Kahn, "Coupled-core multi-core fibers for spatial multiplexing," *IEEE Photon. Technol. Lett.*, vol. 25, no. 21, pp. 2054–2057, Nov. 2013.
[17] C. Antonelli, A. Mecozzi, and M. Shtaif, "The delay spread in fibers for SDM transmission: Dependence on fiber parameters and perturbations," *Opt. Exp.*, vol. 23, no. 3, pp. 2196–2202, Feb. 2015.
[18] A. W. Snyder, "Coupled-mode theory for optical fibers," *J. Opt. Soc. Amer.*, vol. 62, no. 11, pp. 1267–1277, Nov. 1972.
[19] J. P. Gordon and H. Kogelnik, "PMD fundamentals: Polarization mode dispersion in optical fibers," *Proc. Nat. Acad. Sci.*, vol. 97, no. 9, pp. 4541–4550, 2000.
[20] D. Gloge, "Weakly guiding fibers," *Appl. Opt.*, vol. 10, no. 10, pp. 2252–2258, Oct. 1971.
[21] R. E. Schuh, "Theoretical analysis and measurement of effects of fibre twist on polarisation mode dispersion of optical fibres," *Electron. Lett.*, vol. 31, no. 20, pp. 1772–1773, 1995.
[22] R. Ryf *et al.*, "Space-division multiplexed transmission over 4200-km 3-core microstructured fiber," in *Proc. Nat. Fiber Optic Eng. Conf.*, 2012, Art. no. PDP 5C.2. [Online]. Available: http://www.osapublishing.org/abstract.cfm?URI=NFOEC-2012-PDP5C.2
[23] A. Mecozzi, C. Antonelli, and M. Shtaif, "Intensity impulse response of SDM links," *Opt. Exp.*, vol. 23, no. 5, pp. 5738–5743, Mar. 2015.
[24] R. Veronese *et al.*, "Distributed measurement of birefringence in uncoupled multicore fibers," in *Proc. Opt. Fiber Commun. Conf.*, 2021, Art. no. W7B.3. [Online]. Available: http://www.osapublishing.org/abstract.cfm?URI=OFC-2021-W7B.3
[25] A. Pizzinat, B. S. Marks, L. Palmieri, C. R. Menyuk, and A. Galtarossa, "Polarization mode dispersion of spun fibers with randomly varying birefringence," *Opt. Lett.*, vol. 28, no. 6, pp. 390–392, Mar. 2003.
[26] T. Sakamoto *et al.*, "Randomly-coupled single-mode 12-core fiber with highest core density," in *Proc. Opt. Fiber Commun. Conf. Exhib.*, 2017, pp. 1–3.
[27] H. Haus and W. Huang, "Coupled-mode theory," *Proc. IEEE*, vol. 79, no. 10, pp. 1505–1518, Oct. 1991.
[28] L. Palmieri and A. Galtarossa, "Intramodal dispersion properties of step-index few-mode spun fibers," *J. Lightw. Technol.*, vol. 34, no. 2, pp. 303–313, 2016.
[29] C. Antonelli, A. Mecozzi, M. Shtaif, and P. J. Winzer, "Random coupling between groups of degenerate fiber modes in mode multiplexed transmission," *Opt. Exp.*, vol. 21, no. 8, pp. 9484–9490, Apr. 2013.
[30] C. Antonelli, G. Riccardi, T. Hayashi, and A. Mecozzi, "Role of polarization-mode coupling in the crosstalk between cores of weakly-coupled multi-core fibers," *Opt. Exp.*, vol. 28, no. 9, pp. 12 847–12 861, Apr. 2020.
[31] C. Antonelli, A. Mecozzi, M. Shtaif, N. K. Fontaine, H. Chen, and R. Ryf, "Stokes-space analysis of modal dispersion of SDM fibers with mode-dependent loss: Theory and experiments," *J. Lightw. Technol.*, vol. 38, no. 7, pp. 1668–1677, 2020.
[32] R. Dar, M. Feder, A. Mecozzi, and M. Shtaif, "Pulse collision picture of inter-channel nonlinear interference in fiber-optic communications," *J. Lightw. Technol.*, vol. 34, no. 2, pp. 593–607, Jan. 2016.